15. Yang, P., Zhao, D., Margolese, D. I., Chmelka, B. F. & Stucky, G. D. Generalized syntheses of large-pore mesoporous metal oxides with semicrystalline frameworks. *Nature* **396,** 152–155 (1998).
16. Lee, B., Lu, D., Kondo, J. N. & Domen, K. Three-dimensionally ordered mesoporous niobium oxide. *J. Am. Chem. Soc.* **124,** 11256–11257 (2002).
17. Hwang, Y. K., Lee, K.-C. & Kwon, Y.-U. Nanoparticle route to mesoporous titania thin films. *Chem. Commun.* 1738–1739 (2001).
18. Yun, H. S., Miyazawa, K., Zhou, H. S., Honma, I. & Kuwabara, M. Synthesis of mesoporous thin TiO_2 films with hexagonal pore structure using triblock copolymer templates. *Adv. Mater.* **13,** 1377–1380 (2001).
19. Mcmillan, P. W. *Glass-Ceramics* (Academic, London, 1979).
20. Gaskell, P. H. Structure, glass formation and properties. *J. Non-Crystal. Solids* **192/193,** 9–22 (1995).
21. Lu, Y. *et al.* Self-assembly of mesoscopically ordered chromatic polydiacetylene/silica nanocomposites. *Nature* **410,** 913–917 (2001).
22. Inagaki, S., Guan, S., Ohsuna, T. & Terasaki, O. An ordered mesoporous organosilica hybrid material with a crystal-like wall structure. *Nature* **416,** 304–307 (2002).
23. Li, D., Kong, L., Zhang, L. & Yao, X. Sol-gel preparation and characterization of transparent $KTiOPO_4/SiO_2$ nanocomposite glass for second harmonic generation. *J. Non-Cryst. Solids* **271,** 45–55 (2000).
24. James, P. F., Iqbal, Y., Jais, U. S., Jordery, S. & Lee, W. E. Crystallisation of silicate and phosphate glasses. *J. Non-Cryst. Solids* **219,** 17–29 (1997).
25. Pinckney, L. R. & Beall, G. H. Nanocrystalline non-alkali glass-ceramics. *J. Non-Cryst. Solids* **219,** 219–227 (1997).
26. Fujishima, A. & Honda, K. Electrochemical photolysis of water at a semiconductor electrode. *Nature* **238,** 37–38 (1972).
27. O'Regan, B. & Gratzel, M. A low-cost, high-efficiency solar cell based on dye-sensitized colloidal TiO_2 film. *Nature* **353,** 737–739 (1991).
28. Bach, U. *et al.* Solid-state dye-sensitized mesoporous TiO_2 solar cells with high photon-to-electron conversion efficiencies. *Nature* **395,** 583–585 (1998).
29. Wagemaker, M., Kentgens, A. P. M. & Mulder, F. M. Equilibrium lithium transport between nanocrystalline phases in intercalated TiO_2 anatase. *Nature* **418,** 397–399 (2002).
30 Talavera, R. R., Vargas, S., Arroyo-Murillo, R., Montiel-Campos, R. & Haro-Poniatowski, E. Modification of the phase transition temperatures in titania doped with various cations. *J. Mater. Res.* **12,** 439–443 (1997).
31. Schmutz, C. *et al.* EXAFS, Raman and ^{31}P NMR study of amorphous titanium phosphates. *J. Non-Cryst. Solids* **170,** 250–262 (1994).

Acknowledgements

D.L. acknowledges the financial support of the Japanese Society of the Promotion of Science (JSPS) Fellowship for work carried out at the Energy Electronics Institute, AIST. H.Z. thanks M. Ichihara for help in TEM observations, and acknowledges partial research funding from JSPS, Japan Science and Technology Agency, AIST.
Correspondence and requests for materials should be addressed to H. Z.
Supplementary Information accompanies the paper on www.nature.com/naturematerials

Competing financial interests

The authors declare that they have no competing financial interests.

CORRIGENDUM

Synthesis and size-dependent properties of zinc-blende semiconductor quantum rods

SHIHAI KAN, TALEB MOKARI, ELI ROTHENBERG AND URI BANIN

Nature Materials **2**, 155–158 (2003).

In this letter, Fig. 1f and Supplementary Information Fig. S4 were partially wrongly characterized in relation to indexing the growth direction of InAs wires that are found in the precipitate. Both figures are corrected below. We additionally comment that we observed in the powder X-ray diffraction pattern of the precipitate containing InAs wires that the [220] and [311] peaks of InAs are stronger than the [111] peak, unlike the rods (Fig. 3 in the original paper). The strong relative intensity of the [220] peak indicates that the growth of the wires takes place along the <110> direction. This is further supported by the HRTEM image of the wires (Fig. 1f and Supplementary information, Fig. S4). The higher intensity of the [311] peak might be caused by other, non-wire shaped, crystalline InAs structures in this fraction.

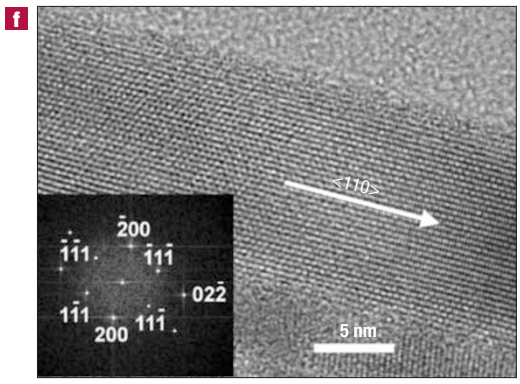

Figure 1f HRTEM image of part of a nanowire with total dimensions 200 × 12 nm. The wire, without stacking faults, grows along the InAs <110> direction. Inset: Fourier transform of the image, indicating that the wire is viewed along the <011> zone axis of the cubic structure.

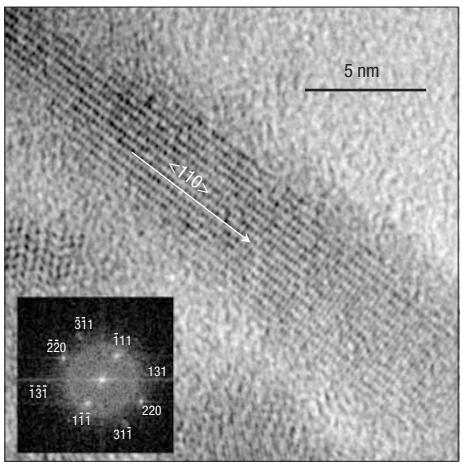

Figure S4 HRTEM of an InAs nanowire, ~200 × 5 nm in size. The wire grows along the [110] direction, as also indicated in the Fourier transform of the image viewed along the <112> zone axis.